J|A|C|S
ARTICLES
Published on Web 09/13/2002

Glycyl C^{α} Chemical Shielding in Tripeptides: Measurement by Solid-State NMR and Correlation with X-ray Structure and Theory

Eduard Y. Chekmenev, Ray Z. Xu, Mark S. Mashuta, and Richard J. Wittebort*

Contribution from the Department of Chemistry, University of Louisville, Louisville, Kentucky 40292

Received April 26, 2002

Abstract: We report here $^{13}C^{\alpha}$ chemical shielding parameters for central Gly residues in tripeptides adopting α-helix, β-strand, polyglycine II, and fully extended 2° structures. To assess experimental uncertainties in the shielding parameters and the effects of $^{14}N-^{13}C^{\alpha}$ or $^{15}N-^{13}C^{\alpha}$ dipolar coupling, stationary and magic angle spinning (MAS) spectra with and without ^{15}N decoupling were obtained from natural abundance and double-labeled samples containing [2-^{13}C, ^{15}N]Gly. We find that accurate (<1 ppm uncertainty) shielding parameters are measured with good sensitivity and resolution in ^{15}N decoupled 1D or 2D MAS spectra of double-labeled samples. Compared to variations of isotropic shifts with peptide angles, those of $^{13}C^{\alpha}$ shielding anisotropy and asymmetry are greater. Trends relating shielding parameters to the 2° structure are apparent, and the correlation of the experimental values with unscaled ab initio shielding calculations has an rms error of 3 ppm. Using the experimental data and the ab initio shielding values, the empirical trends relating the 2° structure to shielding are extended to the larger range of torsion angles found in proteins.

Introduction

Chemical shielding is at the heart of most NMR experiments. At the most rudimentary level, it is the source of resolution which separates lines from chemically different groups. In turn, the correlation of isotropic shifts with chemical connectivity and environment provides numerous insights about chemical properties. With the development of ab initio quantum chemistry, empirical correlations are augmented by a direct comparison of experiment with calculation. For example, the large database of $^{13}C^{\alpha}$ isotropic chemical shifts from solution NMR protein structures indicates a good correlation with the protein 2° structure,[1] and calculations suggest that $^{13}C^{\alpha}$ shielding tensor principal components are largely dependent on the 2° structure, that is, backbone torsion angles (ϕ,ψ).[2,3] On the basis of this idea, a simple strategy for determining 2° structure in randomly oriented polypeptides has been described.[4] Measured shielding tensor principal components for Ala, Val, and Leu residues in small peptides of known structure[5−7] have been determined and compared with calculations.[8] The correlation between theory and experiment is good if the ab initio calculations are scaled.[5] Development of this approach and experimental strategies for exploiting shielding anisotropies,[9] thus, requires an additional experimental determination of $^{13}C^{\alpha}$ shielding tensors in peptides of known structure. The modest experimental database of known $^{13}C^{\alpha}$ shielding tensors has been recently summarized[6] and includes no systematic study of glycyl residues.

Herein, we report such a study of tripeptides containing central glycyl residues. Glycine contains no side chain, eliminating any possible effects of side-chain conformation, and it is a frequently occurring residue in proteins (6.8% of residues in known proteins). Tripeptides studied here have central Gly residues with torsion angles characteristic of α-helices, β-strands, the polyproline/polglycine II collagen structure, and fully extended conformations. We discuss the variation of the shielding tensor parameters ($\delta_{11} - \delta_{33}$) and ($\delta_{22} - \delta_{33}$) with torsion angles and the correlation with published calculations. A noteworthy feature of these results is that the shielding parameters vary over larger ranges than the isotropic shifts. This greater sensitivity is of practical utility in solid-state NMR, where the resolution of the experiment is substantially less than in solution NMR. In addition, it is less demanding of the theoretical shielding calculation.

Several experimental questions regarding accurate measurements of ($\delta_{11} - \delta_{33}$) and ($\delta_{22} - \delta_{33}$) under conditions appropriate for examining larger biomolecules are explicitly

* Address correspondence to this author. E-mail: rjwitt01@athena.louisville.edu.

(1) Wishart, D. S.; Sykes, B. D. *J. Biomol. NMR* **1994**, *4*(2), 171−180.
(2) De Dios, A. C.; Pearson, J. G.; Oldfield, E. *Science* **1993**, *260*, 1491−1496.
(3) De Dios, A. C.; Oldfield, E. *J. Am. Chem. Soc.* **1994**, *116*, 11485−11488.
(4) Heller, J.; Laws, D. D.; Tomaselli, M.; King, D. S.; Wemmer, D. E.; Pines, A.; Havlin, R. H.; Oldfield, E. *J. Am. Chem. Soc.* **1997**, *119*, 7827−7831.
(5) Havlin, R. H.; Laws, D. D.; Bitter, H.-M. L.; Sanders, L. K.; Sun, J. S.; Wemmer, A.; Pines, A.; Oldfield, E. *J. Am. Chem. Soc.* **2001**, *123*, 10362−10369.
(6) Wei, Y.; Lee, D. K.; Ramamoorthy, A. *J. Am. Chem. Soc.* **2001**, *123*, 6118−6126.
(7) Havlin, R. H.; Le, H.; Laws, D.; deDios, A. C.; Oldfield, E. *J. Am. Chem. Soc.* **1997**, *119*, 11951−11958.
(8) Yao, X.; Hong, M.; *J. Am. Chem. Soc.* **2002**, 124, 2730−2738.
(9) Hong, M. *J. Am. Chem. Soc.* **2000**, *122*, 3762−3770.

10.1021/ja026700g CCC: $22.00

addressed by using triple resonance ($^1H/^{13}C/^{15}N$) spectroscopy of stationary and spinning samples with double labeling ([2-^{13}C, ^{15}N]Gly) or at natural abundance. Comparison of ^1H and ^{15}N decoupled stationary and 1-D MAS spectra allows us to assess the accuracy of determining principal components from spinning sideband intensities. The effect of ^{14}N coupling[10] to C^α is studied by comparing ^{15}N decoupled spectra of double-labeled samples with spectra at natural abundance. The latter are sufficiently crowded that a 2-D technique placing isotropic shifts and spinning sidebands in separate dimensions is used. When given the 1.1% natural abundance of ^{13}C, successful application of this technique suggests the feasibility of performing these experiments on proteins containing a limited number of labeled sites.

Experimental Methods

Peptide Synthesis. Peptides studied at natural abundance were obtained from Bachem (King of Prussia, PA). Seven tripeptides with *G = [2-^{13}C, ^{15}N]Gly were prepared (G*GV, G*GG, A*GG, P*GG, F*GG, Y*GG, and V*GG) by solid-phase synthesis. [2-^{13}C, ^{15}N]Glycine was purchased from CIL (Andover, MA) and converted to *t*-Boc-*Gly by reaction with *tert*-butyloxycarbonyl anhydride in *t*-BuOH/NaOH. The product was acidified with HCl/CH_3COOH, extracted with ethyl acetate, and recrystallized.[11] The course of coupling reactions were monitored by reacting a few of the nascent peptide resin beads with ninhydrin and examining their color under a microscope. Reactions were deemed complete when all color (initially purple and later yellow) was absent. An ~1.5-fold excess of *t*-Boc-*Gly was coupled to Gly resin (Chem-Impex International, Wood Dale, IL) using the coupling reagent 1-hydroxybenzotriazole (HOBt) and Castro's reagent (BOP) in DMF. The N-terminal residue was coupled using a 6-fold excess of the *t*-Boc amino acid. Peptides were cleaved from the Merrifield resin with anhydrous HF.[11] The product was extracted with 25% acetic acid and lyophilized. Initial purification was by cation exchange chromatography. A 100−200-mg amount of crude peptide dissolved in 50% acetic acid was applied to a Pasteur pipet containing ~1 g of Dowex 50WX8−100. The column was washed with several volumes of water, and the peptide eluted with 1% NH_4OH. Final purification was by size exclusion chromatography on a 1-m column of Sephadex LH-20 (Amersham Pharmacia Biotech AB, Uppsala, Sweden) in 50% acetic acid. When prepared in this fashion, peptides yielded single spots in silica gel thin-layer chromatography (solvent system H_2O (30%)/C_2H_5OH (70%)), had the expected molecular weights as determined by MALDITOFF mass spectroscopy, and readily crystallized.

NMR Samples. Crystalline samples of the peptides for solid-state NMR (containing 8−25 mg of labeled material) were grown according to the procedures described in the original X-ray literature: G*GG,[12,13] A*GG,[14] P*GG,[15] F*GG,[16] Y*GG,[17] and V*GG,[18] G*GV,[19] WGG.[20] Cambridge Crystal Data Base[21] reference codes for these structures are listed in Table 2.

X-ray Crystallography. The unit cell dimensions and space groups were determined for all of the peptides studied here by X-ray crystallography and conformed to the published values. The complete X-ray structure of one GGG polymorph with cell dimensions and space group equivalent to those of CSD (Cambridge structural database) code TGLYCY10 was determined using a Bruker SMART APEX CCD area detector system at 100 K and standard software.[22−24] A thin, colorless needle ($0.03 \times 0.04 \times 0.31$ mm^3) was determined to be a single crystal. For all 3516 unique reflections (R(int) = 0.032), the final anisotropic full-matrix least-squares refinement on F^2 for 323 variables converged at $R_1 = 0.046$ and w$R_2 = 0.093$ with a GOF of 1.05.

NMR Spectra. ^{13}C NMR spectra were obtained on a home-built 11.7-T instrument (^{13}C Larmor frequency of 124.59 MHz) with 5-mm ($^1H/^{13}C$) double-resonance or 4-mm ($^1H/^{13}C/^{15}N$) triple-resonance MAS probes built on a design previously described.[25] Sample spinning speeds were controlled to within ±3 Hz (Doty Scientific, Columbia, S.C.). ^{13}C spectra were excited by cross-polarization from abundant protons using a 2-ms Hartman−Hahn contact ($\gamma B_1^C/2\pi = \gamma B_1^H/2\pi = 42$ kHz) and accumulated with high power ($\gamma B_1^H/2\pi = 125$ kHz) two pulse phase modulated (tppm) decoupling[26] with recycle times sufficiently long to give equilibrium signal intensities. The tppm phase shift was 22.5°, and line widths were minimized by adjusting the ^1H flip angle (~150°). From spectra obtained in this way, we arrived at the following criteria for an acceptable sample: C^α line widths in the range 50−100 Hz (0.4−0.8 ppm). Samples of WGG and F*GG were doped with $CuSO_4$ to shorten the ^1H T_1. Triple resonance experiments used unmodulated ^{15}N decoupling ($\gamma B_1^N/2\pi = 40$ kHz). The 2-D PASS experiment was implemented on our instrument as described by Anzutkin et al.[27] All ^{13}C spectra were referenced to external adamantane using the more intense, downfield line at 38.6 ppm.

NMR Spectrum Analysis. Principal shielding components were obtained from 1-D and 2-D MAS spectra by the Berger−Herzfeld[28] procedure using computer programs (i) kindly provided by Professor Malcolm Levitt or (ii) written by us. The latter provides a surface of $\chi^2 = (1/\sigma_{noise}^2)\sum(I_j^{exp} - I_j^{calc})^2$ as a function of the two fitting parameters, $(\delta_{11} - \delta_{33})$ and $(\delta_{22} - \delta_{33})$, the covariance matrix, and a Monte Carlo error analysis. The fitting parameters used here were chosen, since they vary continuously for all possible values of δ_{ii}. Visual inspection of the χ^2 surface confirms the optimum fit (global minimum in χ^2) and, if present, shows local minima. With the assumption that experimental errors are dominated by spectrum signal-to-noise (σ_{noise}^2 is the mean square noise amplitude measured directly from the NMR spectrum), standard errors and confidence intervals are determined in three ways:[29,30] (i) from the covariance matrix, (ii) from $\Delta\chi^2 = \chi^2 - \chi_{min}^2$ contours, and (iii) by Monte Carlo simulation. In a Monte Carlo trial, exact sideband intensities corresponding to the best-fit parameters are added to Gaussian random noise with the experimental σ_{noise}^2 and then refitted. On the basis of a large number of trials (~10^3), the range of parameters found provides a good estimate of parameter error limits when the relation between data and parameters is either linear or, as is the case here, nonlinear.[29,30] Source code (Fortran), look-up table and i/o files are available upon request.

(10) Wang, C.; Teng, Q.; Cross, T. A. *Biophys. J.* **1992**, *61*(6), 1550−1556.
(11) Stewart, J. M.; Young, J. D. *Solid-Phase Peptide Synthesis*, 2nd ed.; Pierce Chemical Co.: Rockford, IL, 1984; Chapter 2.
(12) Srikrishnan, T.; Winiewicz, N.; Parthasarathy, R. *Int. J. Pept. Protein Res.* **1982**, *19*, 103−113.
(13) Lalitha, V.; Subramanian, E. *Cryst. Struct. Commun.* **1982**, *11*, 561−564.
(14) Subramanian, E.; Lalitha, V. *Biopolymers* **1983**, *22*, 833−838.
(15) Lalitha, V.; Murali, R.; Subramanian, E. *Int. J. Pept. Protein Res.* **1986**, *27*, 472−477.
(16) Subramanian, E.; Sahayamary, J. *Int. J. Pept. Protein Res.* **1989**, *34*, 211−214.
(17) Carson, W. M.; Hackert, M. L. *Acta Crystallogr., Sect. B:* **1978**, *34*, 1275−1280.
(18) Lalitha, V.; Subramanian, E.; Parthasarathy, R. *Int. J. Pept. Protein Res.* **1986**, *27*, 223−228.
(19) Lalitha, V.; Subramanian, E.; Bordner, J. *Int. J. Pept. Protein Res.* **1984**, *24*, 437−441.
(20) Subramanian, E.; Sahayamary, J. *Int. J. Pept. Protein Res.* **1989**, *34*, 134−138.
(21) Allen, F. H.; Kennard, O. *Chemical Design Automation News* **1993**, *8*(1), 1 and 31−37.
(22) *SHELXTL*, version 6.12; Bruker AXS, Inc.: Madison, WI, 2001.
(23) Sheldrick, G. M. SHELXS-90. *Acta Crystallogr.* 1990, A46, 467.
(24) Sheldrick, G. M. *SHELXL-97: Program for the Refinement of Crystal Structures*; University of Göttingen: Göttingen, Germany, 1997.
(25) Zhang, Q. W.; Zhang, H.; Lakshmi, K. L.; Lee, D. K.; Bradley, C. H.; Wittebort, R. J. *J. Magn. Reson.* **1998**, *132*, 167−171.
(26) Bennett, A. E.; Rienstra, C. M.; Auger, M.; Lakshmi, K. V.; Griffin, R. G. *J. Chem. Phys.* **1995**, *103*, 6951−6958.
(27) Antzutkin, O. N.; Shekar, S. C.; Levitt, M. H. *J. Magn. Reson., Ser. A* **1994**, *115*, 7−19.
(28) Herzfeld, J.; Berger, A. E. *J. Chem. Phys.* **1980**, *73*, 6021−6030.
(29) Press, W. H.; Flannery, B. P.; Teukolsky, S. A.; Vetterling, W. T. *Numerical Recipes*; Cambridge University Press: Cambridge, U.K., 1988.
(30) Bevington, P. R.; Robinson, D. K. *Data Reduction and Error Analysis for the Physical Sciences*, 2nd ed.; McGraw-Hill: New York, 1992.

Table 1. Comparison of $(\delta_{11} - \delta_{33})$ and $(\delta_{22} - \delta_{33})$ Determined by Different Methods

sample	method	decoupling	*S/N*[a]	No. of sb's	$(\delta_{11} - \delta_{33})^{b,c}$	$(\delta_{22} - \delta_{33})^{b,c}$
A*GG	powder	^{1}H/^{15}N	166		51.5(1.5)	23.7(1.5)
A*GG	MAS	^{1}H/^{15}N	137	9	53.1(0.4)	24.8(0.5)
G*GV	powder	^{1}H/^{15}N	120		48.5(1.5)	18.3(1.5)
G*GV	MAS	^{1}H/^{15}N	90	7	48.9(0.6)	20.3(0.8)
P*GG	powder	^{1}H/^{15}N	150		50.5(1.5)	21.8(1.5)
P*GG	MAS	^{1}H/^{15}N	127	9	50.7(0.7)	22.0(0.7)
A*GG	MAS	^{1}H	130	9	52.6(0.4)	26.0(0.5)
AGG	MAS	^{1}H	39	7	51.1(1.0)	25.6(1.7)
AGG	2D-PASS	^{1}H	29	7	50.4(1.2)	25.8(1.8)
G*GV	2D-PASS	^{1}H/^{15}N	100	8	49.3(0.8)	20.9(0.8)
GGV	2D-PASS	^{1}H	45	7	48.3(1.1)	22.8(1.3)
F*GG	MAS	^{1}H/^{15}N	110	7	49.1(0.6)	22.8(0.9)
FGG	2D-PASS	^{1}H	43	7	49.7(1.6)	23.9(1.8)

[a] Spectrum signal-to-noise ratio, *S/N*, is for the centerband. [b] Joint 95% confidence limits are in parentheses. [c] Shielding parameters are in ppm relative to TMS with the convention that $\delta_{11} > \delta_{22} > \delta_{33}$.

Table 2. Shielding Tensor Data for Central Gly Residues

peptide	CSD code	~2° structure[b]	(ϕ,ψ)	δ_{iso}[a,c]	$\delta_{11} - \delta_{33}$[a,c]	$\delta_{22} - \delta_{33}$[a,c]
G*GG	TGLYCY10	extended	178, −172 −165, 175	42.4(0.2)	43.3(0.4)	19.7(0.4)
G*GG	BIBRUZ	anti-β	−153, 160	43.3(0.4)	35.2(0.7)	26.0(0.7)
V*GG	COPBIS10	anti-β	−155, 155	43.0(0.2)	34.7(0.6)	25.0(0.6)
P*GG	FABXUB10	3_1-helix	−71, 167	43.0(0.2)	50.7(0.5)	22.0(0.5)
A*GG	CALXES20	3_1-helix	−83, 169	42.9(0.2)	53.0(0.7)	24.9(0.7)
F*GG	FIZWIU01	α_R-helix	−90, −29	44.5(0.4)	49.1(0.6)	22.8(0.9)
G*GV	CUWRUH	α_R-helix	−77, −22	44.8(0.2)	48.9(0.6)	20.3(0.8)
WGG	FIZWOA01	α_L-helix	88, 10	44.3(0.2)	50.3(5)	25.0(5)
Y*GG	LTYRGG10	α_L-helix	81, 12	44.2(0.2)	41.3(0.5)	16.3(0.6)

[a] Numbers in parentheses are 95% joint confidence intervals. [b] α_R-helix and α_L-helix are right and left-handed α-helices. [c] Shielding parameters are in ppm relative to TMS.

Results

With the goal of measuring chemical shielding parameters in proteins, essential practical considerations are sensitivity, resolution, and the reliability of the shielding values. We investigate these by summarizing results obtained with several peptides using stationary and spinning samples and different decoupling schemes with labeled and unlabeled samples, Table 1. Experiments, for example, with and without ^{13}C, ^{15}N labeling of the central Gly residue allow a direct assessment of the effects of dipolar coupling between C^α and bonded ^{14}N or ^{15}N. Shielding parameters are listed in terms of $(\delta_{11} - \delta_{33})$ and $(\delta_{22} - \delta_{33})$ with the convention that δ_{11} and δ_{33} are, respectively, the most downfield and upfield components. Note that these two parameters with the isotropic shift, δ_{iso} (Table 2), determine the three shielding tensor principal components. The value of $(\delta_{11} - \delta_{33})$ gives the overall breadth of chemical shielding, while $(\delta_{22} - \delta_{33})$ is closely related to the asymmetry parameter, η. When $(\delta_{22} - \delta_{33})$ vanishes or equals $(\delta_{11} - \delta_{33})$, the tensor is axial, $\eta = 0$, or when $(\delta_{22} - \delta_{33})/(\delta_{11} - \delta_{33}) = {}^1/_2$, $\eta = 1$.

In simple cases (nonoverlapping powder patterns and absence of dipolar couplings), shielding tensor principal components are determined from powder patterns by inspection of the turning points or by line shape fitting. Alternatively, Berger−Herzfeld analysis of MAS sideband intensities[28] provides a substantial resolution advantage, albeit at the possible expense of determining principal component frequencies via line intensities. The accuracies are tested by standard error analysis of the values determined by both methods.

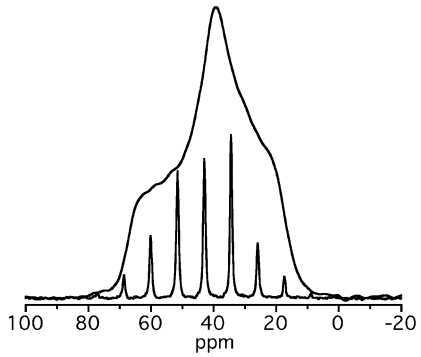

Figure 1. Powder and MAS ($\nu_r = 1.1$ kHz) ^{1}H, ^{15}N decoupled ^{13}C spectra of P*GG. Spectra were obtained with 2048 and 720 transients, respectively.

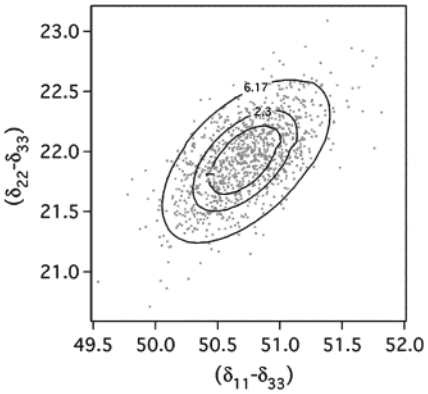

Figure 2. $\Delta\chi^2$ contours obtained from the least-squares fitting of the P*GG MAS spectrum and parameter values (gray dots) from 10^3 Monte Carlo trials simulating the effect of experimental noise on the fitted parameters.

Figure 1 shows the ^{15}N/^{1}H decoupled ^{13}C powder and MAS spectra of P*GG, wherein the observed spectral patterns are determined by the C^α chemical shielding alone.

Best fit values of the shielding parameters, *S/N* values, and confidence intervals are listed in Table 1. Importantly, the $\Delta\chi^2$ surface shows a single minimum, indicating that the shielding parameters are uniquely determined by the MAS spectrum. To specify confidence limits in the fitted shielding parameters, three $\Delta\chi^2$ contours for the P*GG MAS data and the results of the Monte Carlo simulation are superposed in Figure 2.

Shown are frequently used contours for 68.4% confidence for individual ($\Delta\chi^2 = 1$) or joint ($\Delta\chi^2 = 2.3$) parameter values as well as the 95% joint confidence level ($\Delta\chi^2 = 6.17$).[29,30] Individual parameter confidence intervals determined by the limits of the $\Delta\chi^2 = 1$ contour are in good agreement with standard errors from the covariance matrix and the individual parameter distributions found in the Monte Carlo simulation. However, the latter shows that parameter values consistent with the experimental noise level frequently vary over a larger range when viewed in the two parameter space shown in Figure 2. Thus, confidence limits listed in Tables 1 and 2 for MAS spectra are at the 95% joint confidence level ($\Delta\chi^2 = 6.17$). Parameter accuracy from stationary powder spectra is limited by spectral resolution; the reciprocal of the spectrum acquisition time[31] which is limited in practice by the time in the acquisition period

(31) Farrar, T. C.; Becker, E. D. *Pulse and Fourier transform NMR; Introduction to Theory and Methods*; Academic Press: New York, 1976.

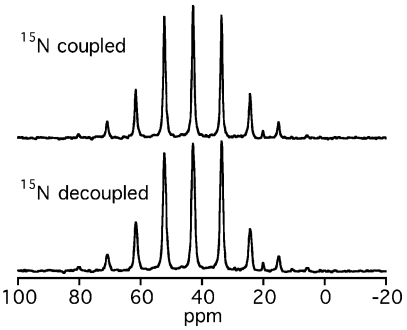

Figure 3. ^{15}N decoupled (256 transients) and coupled (132 transients) ^{13}C MAS ($\nu_r = 1.2$ kHz) spectra of A*GG. The small signal at 20 ppm is a natural abundance Ala methyl group signal.

at which the free induction signal disappears into the noise, ~2 ms in these experiments. This corresponds to a spectral resolution of ±1.5 ppm for the powder patterns. For the three cases where both powder and MAS spectra of double-labeled samples were obtained (P*GG, A*GG and G*GV), the shielding parameters agree within the stated confidence limits. However, in all cases, the MAS parameters are larger than those from the stationary experiment. This is likely due to the lower spectral resolution of the stationary sample experiment, wherein broadening of the powder pattern shoulders results in overestimating δ_{33} and underestimating δ_{11}. In the data reported here, with *S*/*N* ≈ 125:1 and 7 or more sidebands, the MAS experiment is superior to the stationary sample experiment, wherein accuracy is limited by lower spectral resolution.

Spectra of Cα shielding are affected by dipolar coupling with the bonded ^{15}N or ^{14}N.[6,10] We now consider dipolar effects in MAS experiments. The effect of the quadrupole mixing of ^{14}N Zeeman states on a dipolar coupled spin $^1/_2$ spectrum in MAS NMR has been quantitatively explained.[32] MAS lines appear as 2:1 doublets with a maximum splitting of $9\nu_D(e^2qQ/h)/20\nu_0$. Using representative values (N−Cα bond length of 1.47 Å, amide ^{14}N quadrupole coupling of 3.2 MHz,[33] and NMR frequency of 35.8 MHz), this splitting is ~28 Hz, a value 2- or 3-fold less than the line widths observed here. This expectation is experimentally confirmed, that is, no such splittings were observed in numerous spectra of unlabeled peptides.

Consequently, ^{13}Cα sideband intensities at the field used here (11.7 T) are determined by a combination of first-order chemical shielding ($H^{cs} = \sigma I_z$) and dipolar coupling ($H^{dipole} = DI_zS_z$). For the standard N−Cα bond length 1.47 Å, the dipolar coupling, ν_D, is 690 Hz or 5.5 ppm for ^{14}N and 960 Hz or 7.7 ppm for ^{15}N. Although these couplings are 10−15% of ($\delta_{11} - \delta_{33}$) at 11.7 T, MAS spectra at $\nu_r = 1.2$ kHz with and without ^{15}N decoupling, Figure 3, and the shielding parameters obtained by neglecting dipolar coupling, Table 1, show only a small effect.

Only ($\delta_{22} - \delta_{33}$) is systematically different (larger by 1.2 ppm) in the absence of ^{15}N decoupling when ^{15}N coupling is neglected in the fitting procedure. This observation is quantitatively simulated as follows: compared to the MAS experiment involving only chemical shielding, the shielding tensor, σ, is replaced by "effective" tensors, $\sigma_{eff}(m_S) = \sigma + m_S\mathbf{D}$, for the two or three nitrogen spin states ($m_S = \pm^1/_2$ for ^{15}N or $m_S = 0$, ±1 for ^{14}N).[34] **D** is the traceless, axially symmetric dipole tensor with the unique component ν_D along the C−N bond and expressed in the same frame as σ. Consequently, the observed MAS spectrum is a sum of center and sideband intensities resulting from two or three "effective" tensors. While the effect of dipolar coupling is apparent in simulations with $\nu_r \ll \nu_D$, with $\nu_r = 1.2$ kHz, simulated changes in sideband intensities are a few percent as experimentally observed, Figure 3.

When compared to ^{15}N, the effect of dipolar coupling to ^{14}N is potentially larger (ν_D for ^{14}N is smaller but m_s takes on values 2-fold larger). This probably has no observable effect in larger, hydrated peptides where efficient ^{14}N relaxation results in self-decoupling.[10] For tripeptides, we have observed self-decoupling of the amide ^{2}H−^{14}N dipolar coupling ($\nu_D = 1200$ Hz) in one case (GAL) but not in GGV where the Gly_2 amide coupling is seen.[35] Thus, Gly_2 amide ^{13}Cα−^{14}N dipolar coupling likely explains the systematically larger (1.9 ppm) value of ($\delta_{22} - \delta_{33}$) measured in GGV as compared to the ^{15}N decoupled MAS value observed in G*GV.

Regarding the measurement of shielding parameters, we conclude by noting that parameters measured by the 2D experiment are equivalent to those measured in the 1D experiment (Table 1; A*GG, F*GG, and G*GV examples). Furthermore, since it is a constant time 2D experiment,[27] the only increase in total spectrum acquisition time relative to the that of the 1D experiment is from the modest reduction in signal (~20%) that we observe in practice from the sequence used to encode sideband dependent phase. Thus, the resolution advantage of the 2D experiment comes at no cost in accuracy or acquisition time. The 2D spectra with sufficient *S*/*N* are obtained from tripeptides at natural abundance, indicating that the approach can be used for labeled proteins. Shielding parameters are most reliably determined using triple resonance 1D or 2D MAS with double-labeled samples, wherein error limits in the shielding parameters are determined by spectrum signal-to-noise. For example, if the center band *S*/*N* ratio is in excess of 100:1 and the spinning speed is sufficiently slow, $\nu_r < 4(\delta_{11} - \delta_{33})\nu_0$, shielding parameters are determined within 1 ppm. Without ^{15}N decoupling and double-labeled samples, only ($\delta_{22} - \delta_{33}$) appears to be altered and by a small amount (1−2 ppm). An alternative to ^{15}N labeling and decoupling is to use a higher magnetic field (>18 T) and spinning speed such that dipolar coupling is insignificant relative to both shielding and the spinning speed.

The main results presented here are summarized in Table 2. Shielding parameters were obtained with ^{15}N decoupled MAS spectra of samples with [2-^{13}C, ^{15}N]Gly in the central residue with one exception, WGG. Because of limited *S*/*N* in the WGG spectrum, error limits are larger than dipolar effects and we anticipate that the parameters are reliable within these limits. The (ϕ,ψ) angles for the central residues, on the basis of the X-ray coordinates, are listed, and the 2° conformation is labeled according to the standard structure with which it most closely corresponds. Commonly accepted (ϕ,ψ) values are left-handed α-helix (−62°, −41°), right-handed α-helix (57°, 47°), parallel β-strands (−119°, 113°), antiparallel β-strands (−139°, 135°), and 3_1 helix/polyglycine II (−80°, 150°).[36] Table 2 provides examples reasonably close to each of these. The most repre-

(32) Oliveri, A. C.; Frydman, L.; Diaz, L. E. *J. Magn. Reson.* **1987**, *75*, 50−62.
(33) Rabbani, S. R.; Edmonds, D. T.; Gosling, P.; Palmer, M. H. *J. Magn. Reson.* **1987**, *72*, 230−237.
(34) Tycko, R.; Weliky, D. P.; Berger, A. E. *J. Chem. Phys.* **1996**, *105*, 7915−7930.
(35) Pometun, M. S.; Usha, M. G.; Richardson, J. F.; Wittebort, R. J. *J. Am. Chem. Soc.* **2002**, *124*, 2345−2351.

sentative are the β-strand (V*GG and G*GG) and 3_1 helix/polyglycine II (A*GG and P*GG) examples, since both torsion angles fall within 20° of standard values. G*GG is also studied in a fully extended polymorph (CSD code TGLYCY10), and the shielding parameters are quite different from those of the β-strand form. Thus, conformation can have a strong effect on chemical shielding. This sample did not, as might be expected, show distinct isotropic $^{13}C^{\alpha}$ shifts for the central Gly residues of the two molecules in the asymmetric unit. Because of this observation and the difficulties described in obtaining the published structure,[12] the X-ray structure was reinvestigated. An excellent, low temperature (100 K) structure ($R_1 = 0.046$) was obtained that confirmed the published structure (see Experimental Methods). Moreover, to confirm the equivalence of the materials used for the NMR and X-ray experiments, we reproduced the NMR results using a separately recrystallized sample of G*GG and a natural abundance sample (GGG) which shows, in addition to the $^{13}C^{\alpha}$ signal of the labeled sample, four additional $^{13}C^{\alpha}$ lines confirming the presence of two nonequivalent molecules (at the terminal Gly residues) in the NMR samples. For α-helices, examples of both left- and right-handed helices were studied. Since Gly is not chiral, shielding is independent of the helix handedness.[7] The torsion angles conform less closely to the ideal values but are within 35° of ideal α-helix values. This point is further addressed in the Discussion.

Table 2 yields three trends relating glycyl shielding parameters to the 2° structure. (i) Without exception, isotropic shifts, δ_{iso}, for α-helix residues are downfield from β-strand residues with an average shift of 1.5 ppm. This is in agreement with the chemical shift index.[1] Additionally, we observe that 3_1-helix/polyGly II isotropic shifts are in the range observed for β-strands. (ii) The range of anisotropies, $(\delta_{11} - \delta_{33})$, vary from 34.7 ppm (VGG, β−strand) to 53.0 ppm (PGG, 3_1 helix), an order of magnitude larger than the range of isotropic shifts. In terms of 2° structures, 3_1 helices are largest (50.7 and 53.0 ppm), α-helices are intermediate (41.3 to 50.3 ppm), and β-strands are the smallest (34.7 and 35.2 ppm). (iii) A third parameter distinguishing 2° structures is the ratio $(\delta_{22} - \delta_{33})/(\delta_{11} - \delta_{33})$, which is less than $^1/_2$ for both α-helix and 3_1-helix/polyGly II residues but greater than $^1/_2$ for β−strands.

Discussion

The data presented here sample glycyl residues in a variety of backbone conformations close to α-helix, β-strand, 3_1-helix/polyGly II, and fully extended 2° structures. Using MAS triple resonance spectroscopy, accurate shielding parameters have been measured. The observed chemical shielding parameters show consistent results as follows: the β-strand examples have upfield $\delta_{iso} \approx 43$ ppm, small $(\delta_{11} - \delta_{33}) \approx 35$ ppm, and $(\delta_{22} - \delta_{33})/(\delta_{11} - \delta_{33}) > {}^1/_2$; the 3_1-helix/polyGly II examples have upfield $\delta_{iso} \approx 43$ ppm, large $(\delta_{11} - \delta_{33}) \approx 52$ ppm, and $(\delta_{22} - \delta_{33})/(\delta_{11} - \delta_{33}) < {}^1/_2$; while right- and left-handed α-helix examples have downfield $\delta_{iso} \approx 44.5$ ppm, intermediate $(\delta_{11} - \delta_{33}) \approx 41-50$ ppm, and $(\delta_{22} - \delta_{33})/(\delta_{11} - \delta_{33}) < {}^1/_2$. The downfield isotropic shifts for α-helix relative to β-strand residues are in the range observed previously in numerous cases, while the experimental observation of trends for $(\delta_{11} - \delta_{33})$ and $(\delta_{22} - \delta_{33})$ in glycyl residues is new.

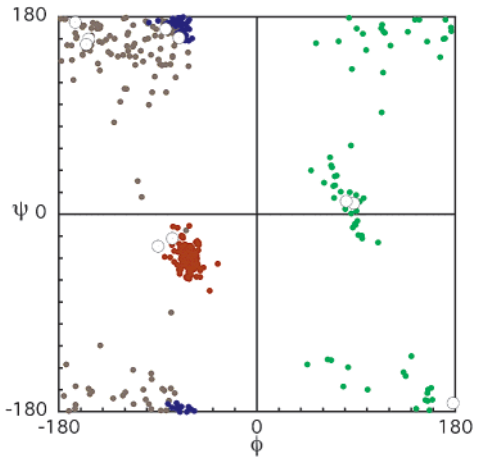

Figure 4. Ramachandran plot showing torsion angles for Gly residues in the peptides studied here (open circles) and Gly residues found in proteins with α-helical (red), β-sheet (brown and green), and the 3_1-helix/polyglycine II (blue) conformations.

When given the small size of the NMR data set, an important question is whether these observations extend beyond the data presented here. In Figure 4, torsion angles on a Ramachandran plot for the peptides studied here (open circles) are compared with those observed for Gly residues from a randomly selected set of proteins in the Protein Data Bank.[37]

Figure 4 includes 208 examples of Gly residues found in α-helices (red) and a similar number found in β-strands (brown and green). Due to a limited number of collagen-like examples in the protein database, the 3_1-helix/polyglycine II set (blue) is smaller (53 examples). We note that an initial set of examples half as large covered the same overall space on the plot.

The tripeptide examples of α-helix and 3_1-helix/polyGly II conformation are representative of the torsion angles found for Gly residues in proteins. Moreover, the regions of a Ramachandran plot occupied by Gly in α-helices and 3_1-helices are well localized. In contrast, the well-known conformational variability of Gly in proteins is displayed only in β-strands. In addition to examples in a somewhat expanded normal range for β-strands (brown), there are numerous examples outside the normal space (green) in which the sign of ϕ is positive. Thus, while the experimental rules concluded above are useful guidelines for identifying α- and 3_1-helix/polyGly II residues, either a much larger set of shielding data or reliable calculations are necessary to identify β-strands by shielding parameters.

To circumvent the need for a large data set, we compare our experimental values, Table 2, with the calculations of Oldfield and co-workers for a tripeptide-like fragment, *N*-formyl glycyl amide.[7] This type of comparison has been made previously for Ala, Val, and Leu residues.[5] When comparing this nonionic fragment and a tripeptide, two obvious questions arise: the effects of charges at the peptide termini and different flanking residues. First, even though most of the peptides studied here are zwitterionic, we anticipate that the comparison is relevant, since termini charges appear to have only a small effect on C^{α} shifts at the adjacent residues. In the case of isotropic shifts, this was noted some time ago[38] in peptides of the form GGXGG

(36) Creighton, T. E. *Proteins: Structures and Molecular Properties*, 2nd ed.; W. H. Freeman: New York, 1993; Chapter 5, p 183.

(37) Berman, H. M.; Westbrook, J.; Feng, Z.; Gilliland, G.; Bhat, T. N.; Weissig, H.; Shindyalov, I. N. Bourne, P. E. *Nucleic Acids Res.* **2000**, *28*, 235−242. Available at www.rcsb.org/pdb/.

(38) Keim, P.; Vigna, R. V.; Marshall, R. C.; Gurd, F. R. N. *J. Biol. Chem.* **1973**, *248*, 6104−6113.

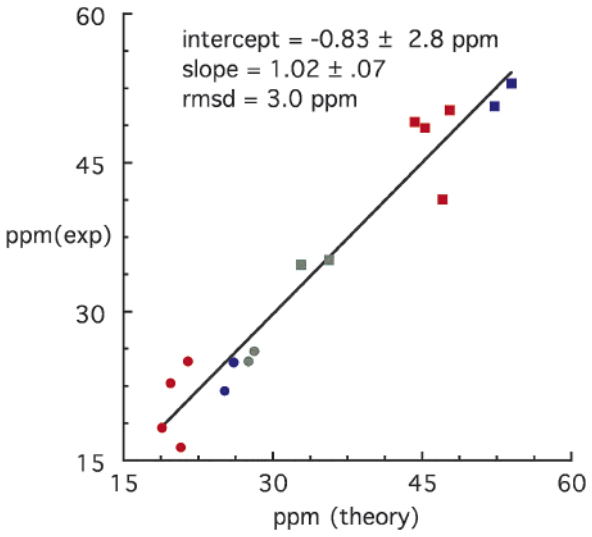

Figure 5. Correlation of experimental, Table 2, and theoretical[7] shielding parameters, $\delta_{22} - \delta_{33}$ (circles) and $\delta_{11} - \delta_{33}$ (squares), respectively. Points are color coded as follows: α-helix (red), β-sheet (green), and the 3_1-helix/polyglycine II (blue) conformations.

where Cα shifts of the central three residues are unchanged in the low pH cationic, neutral pH zwitterionic, and high pH anionic forms. Second, isotropic shifts of the Gly residues flanking the variable X residue vary by less than 0.2 ppm for all residues except X = pro, in which case the shift is 0.8 ppm at the N-terminal side. These observations are also indicated in the anisotropic shielding parameters in two peptides studied here. The hydrogen chloride salts of GGG (BIBRUZ) and zwitterionic VGG have different charges at the termini and different sequences but the same conformation at the central Gly residue, and we observe equivalent shielding parameters. In Figure 5, Table 2 values of $(\delta_{11} - \delta_{33})$ and $(\delta_{22} - \delta_{33})$ are correlated respectively with $(\sigma_{33} - \sigma_{11})$ and $(\sigma_{33} - \sigma_{22})$ values interpolated from the published Gly shielding surface.[7,39]

By correlating shielding differences, $(\delta_{11} - \delta_{33})$ and $(\delta_{22} - \delta_{33})$, we eliminate the need to establish a common reference for theory and experiment. The largest deviations are for α-helix residues, and outliers in the data from the fully extended GGG polymorph (CSD code TGLYCY10) have been eliminated. Unlike the correlation for Ala and Leu where an empirical scaling (0.72−0.84) of the ab initio values was required to bring theory and experiment within reasonable agreement,[5] no scaling is needed or would improve the agreement between theory and experiment for Gly. The rmsd error, 3.0 ppm, is modest in comparison to the properties correlated, indicating a good correlation between theory and experiment ($\rho^2 = 0.97$). Correlating isotropic shifts is less successful ($\rho^2 = 0.74$, rmsd = 0.5 ppm) and requires scaling of the theoretical shifts by 0.82. We conclude that in most cases calculated values of $(\delta_{11} - \delta_{33})$ and $(\delta_{22} - \delta_{33})$ are reliable within several ppm.

The single outlier in the above correlation is the GGG polymorph (CSD code TGLYCY10), which contains two molecules in similar, fully extended conformations. For these two conformations, a single isotropic shift is observed with $(\delta_{11} - \delta_{33}) = 43.3(0.4)$ ppm, a value substantially different from values interpolated from the ab initio surface,[38] 34.2 and 36.0 ppm. As described in the Results section, both the NMR results and the X-ray structure were confirmed. We note that for nearby torsion angles in the area of (−150, 175), shielding parameters vary substantially and include those experimentally observed. Also, sparseness of ab initio calculations near the fully extended conformation[7,38] is a potential source of the disagreement.

In summary, the following generalizations are consistent with this experimental and the published theoretical[7] studies of Gly Cα chemical shielding. In most cases, $(\delta_{11} - \delta_{33})$ values distinguish between α-helix (∼32 ppm to ∼50 ppm) and 3_1-helix/polyGly II (∼45 ppm to ∼55 ppm), but neither is separated from β-strands which displays a wide range of values (∼24 ppm to ∼58 ppm) because of the wide range of torsion angles. In terms of $(\delta_{22} - \delta_{33})/(\delta_{11} - \delta_{33})$, α-helix (∼0.25 to ∼0.4) and 3_1-helix/polyGly II (∼0.35 to ∼0.55) are again easily distinguished, as is, in most cases, α from β (∼0.35 to ∼0.90). Finally, if $(\delta_{22} - \delta_{33})/(\delta_{11} - \delta_{33}) > 0.5$, the structure is β.

The results presented here show that measurements of Gly $^{13}C^{\alpha}$ shielding parameters by MAS spectroscopy are a viable experimental technique for qualitative investigations of 2° structures in proteins. Attractive cases include proteins not amenable to crystallization or solubilization in their native state. Examples are collagens, elastins, and plaques associated with a variety of connective tissue and neurodegenerative diseases. In all of these cases, determination of the 2° structure is important and currently difficult. Also, the $^{13}C^{\alpha}$ shielding parameters reported here should serve as experimental tests for developing improved ab initio calculations. The use of triple resonance and double-labeled samples not only place dipolar coupling to the bonded nitrogen under experimental control but also makes $^{15}N/^{13}C$ resolved spectroscopy possible and ^{15}N shielding parameters available. These would further improve resolution, make the approach more robust, and resolve ambiguities in cases where ^{13}C shielding parameters do not correspond to a unique set of torsion angles or 2° structure. Results of ^{15}N shielding in these peptides will be reported separately.

Acknowledgment. This research was supported by NIH Grant AR41751-07. We thank the Kentucky Research Challenge Trust Fund for the purchase of the CCD X-ray instrument.

JA026700G

(39) Shift Calculator, Eric Oldfield web page. http://feh.scs.uiuc.edu/.